molecules

MDPI

Article

New Polymethoxyflavones from *Hottonia palustris* Evoke DNA Biosynthesis-Inhibitory Activity in An Oral Squamous Carcinoma (SCC-25) Cell Line

Jakub W. Strawa [1], Katarzyna Jakimiuk [1], Łukasz Szoka [2], Krzysztof Brzezinski [3], Paweł Drozdzal [3], Jerzy A. Pałka [2] and Michał Tomczyk [1,*]

[1] Department of Pharmacognosy, Faculty of Pharmacy with the Division of Laboratory Medicine, Medical University of Białystok, ul. Mickiewicza 2A, 15-230 Białystok, Poland; jakub.strawa@umb.edu.pl (J.W.S.); katarzyna.jakimiuk@umb.edu.pl (K.J.)
[2] Department of Medicinal Chemistry, Euroregional Center of Pharmacy, Faculty of Pharmacy with the Division of Laboratory Medicine, Medical University of Białystok, ul. Mickiewicza 2D, 15-222 Białystok, Poland; lukasz.szoka@umb.edu.pl (Ł.S.); pal@umb.edu.pl (J.A.P.)
[3] Department of Structural Biology of Prokaryotic Organisms, Institute of Bioorganic Chemistry, Polish Academy of Sciences, ul. Noskowskiego 12/14, 61-074 Poznań, Poland; kbrzezinski@ibch.poznan.pl (K.B.); pdrozdzal@ibch.poznan.pl (P.D.)
* Correspondence: michal.tomczyk@umb.edu.pl; Tel.: +48-85-748-56-94

Abstract: Four new compounds, 5-hydroxy-2′,6′-dimethoxyflavone (**4**), 5-hydroxy-2′,3′,6′-trimethoxyflavone (**5**), 5-dihydroxy-6-methoxyflavone (**6**), and 5,6′-dihydroxy-2′,3′-dimethoxyflavone (**7**), and three known compounds, 1,3-diphenylpropane-1,3-dione (**1**), 5-hydroxyflavone (**2**), and 5-hydroxy-2′-methoxyflavone (**3**), were isolated from the aerial parts of *Hottonia palustris*. Their chemical structures were determined through the use of spectral, spectroscopic and crystallographic methods. The quantitative analysis of the compounds (**1–7**) and the zapotin (**ZAP**) in methanol (**HP1**), petroleum (**HP6**), and two chloroform extracts (**HP7** and **HP8**) were also determined using HPLC-PDA. The biological activity of these compounds and extracts on the oral squamous carcinoma cell (SCC-25) line was investigated by considering their cytotoxic effects using the MTT assay. Subsequently, the most active compounds and extracts were assessed for their effect on DNA biosynthesis. It was found that all tested samples during 48 h treatment of SCC-25 cells induced the DNA biosynthesis-inhibitory activity: compound **1** (IC_{50}, 29.10 ± 1.45 μM), compound **7** (IC_{50}, 40.60 ± 1.65 μM) and extracts **ZAP** (IC_{50}, 20.33 ± 1.01 μM), **HP6** (IC_{50}, 14.90 ± 0.74 μg), **HP7** (IC_{50}, 16.70 ± 0.83 μg), and **HP1** (IC_{50}, 30.30 ± 1.15 μg). The data suggest that the novel polymethoxyflavones isolated from *Hottonia palustris* evoke potent DNA biosynthesis inhibitory activity that may be considered in further studies on experimental pharmacotherapy of oral squamous cell carcinoma.

Keywords: *Hottonia palustris*; Primulaceae; polymethoxyflavones; SCC-25; HPLC-PDA

check for updates

Citation: Strawa, J.W.; Jakimiuk, K.; Szoka, Ł.; Brzezinski, K.; Drozdzal, P.; Pałka, J.A.; Tomczyk, M. New Polymethoxyflavones from *Hottonia palustris* Evoke DNA Biosynthesis-Inhibitory Activity in An Oral Squamous Carcinoma (SCC-25) Cell Line. *Molecules* **2022**, *27*, 4415. https://doi.org/10.3390/molecules27144415

Academic Editors: M. Mizerska-Kowalska, Wojciech Płaziński, Sylwia Sowa and Roman Paduch

Received: 8 June 2022
Accepted: 6 July 2022
Published: 10 July 2022

1. Introduction

Cancer contributed to 10 million deaths in 2020. The International Agency for Research on Cancer indicates a nearly 50% increase in the incidence of carcinoma, with oral tumors being responsible for almost 380,000 cancer cases and 180,000 deaths per year [1]. The secondary metabolites of higher plants remain an important source of cytostatic and cytotoxic substances as well as non-toxic substances with preventive effects [2]. Vincristine, paclitaxel, and homoharringtonine have been successfully used in medicine, and nearly a hundred new substances are in the clinical trial stage [3]. Due to the multidirectional action of flavonoids, they are considered to be compounds that can play a large role in anticancer therapy [4–6]. Considering a certain range of selectivity, flavonoids, including flavones, have shown in vivo and in vitro activities against tongue squamous carcinoma. Among others, apigenin, baicalein, and naringenin have shown cell cycle inhibition in the G0/G1 phase. In contrast, flavane-3-ol derivatives such as

epigallocatechin gallate (EGCG), epicatechin gallate (ECG), and epigallocatechin (EGC) have shown tumor cell growth inhibition and the activation of apoptosis [7].

Hottonia palustris L. (Primulaceae) (syn.: featherfoil, water violet, Wasserprimel) is a relatively undemanding semiaquatic plant that is widely distributed throughout the lowlands of Western Europe and northern Asia. It grows in calm, shallow waters, ponds, and ditches, mainly forming compact phytocenosis *Hottonietum palustris* [8]. Phytochemical and pharmacological data about *H. palustris* are scarce, and thus, this justifies the need for a more accurate investigation of the chemical constituents and the plant's possible biological targets. The latest literature data mention the presence of saponins [9]. It has been used in folk medicine to treat various diseases, e.g., heart problems [10]. Water violet flowers are also used in the production of Bach's medicinal essences [11]. Moreover, compounds **2**–**4** showed a moderate ability to inhibit tyrosinase activity (IC_{50} 120–127 μM) [12]. The results presented in this study represent an approach for searching for new anticancer agents. Therefore, the aim of this study was to take advantage of the potentialities of spectroscopic, spectrometric and crystallographic methods by applying them to the characterization and structural elucidation of flavones derivatives in *H. palustris* while paying attention to the determination of the methoxylation position in some compounds with the use of and 2D NMR data. To the best of our knowledge, four of them are new natural compounds occurring in the plant kingdom. The quantitative characterization of individual derivatives in extracts is completed with the bioassay-guided assessment of the cytotoxic effect and inhibition of DNA synthesis in tumor cells.

2. Results and Discussion

2.1. Structural Elucidation of Dibenzoylmethane and 5-Hydroxyflavone Derivatives

In previous analyses, the presence of numerous representatives of the polyphenol group in *H. palustris* herb extract was found via the LC-MS method, with the extract mainly including polymethoxyflavones [13,14]. The first attempts to isolate the compounds were made. To ensure high-quality spectroscopic and spectral analyses, all of the compounds were converted into their crystal forms. Then, a series of experiments was performed using compound analysis with ultraviolet light (UV-Vis), high-resolution mass spectrometry (HRMS), and X-ray diffraction assessments. The final determination of the molecule structure was carried out on the basis of one-dimensional (^{1}H, ^{13}C, DEPT) and two-dimensional (COSY, ROESY, HMBC, HSQC, HMQC) nuclear magnetic resonance (NMR). A summary of the signal shift values is presented in Table 1.

Table 1. ^{1}H and ^{13}C spectral data of compounds **4**–**7** (400 Hz for ^{1}H and 100 Hz for ^{13}C spectrum, δ in ppm, J in Hz).

C No.	**4** [A]		**5** [A]		**6** [B]		**7** [B]	
	δ C	δ H	δ C	δ H	δ C	δ H	δ C	δ H
2	162.15	-	161.71	-	163.08	-	162.61	-
3	113.47	6.36, *s*	113.13	6.38, s	112.68	6.4, s	112.34	6.46, s
4	183.74	-	183.55	-	183.01	-	182.91	-
5	160.83	-	160.86	-	159.96	-	159.97	-
6	110.76	6.8 (dd, *J* = 8.03, 0.75)	110.95	6.81 (dd, *J* = 8.28, 0.75)	110.76	6.83 (dd, *J* = 8.5, 0.85)	110.86	6.84 (d, *J* = 8.28)
7	134.9	7.51 (t, *J* = 8.28)	135.07	7.52 (t, *J* = 8.28)	135.91	7.65 (t, *J* = 8.3)	136.0	7.67 (t, *J* = 8.5)
8	107.26	6.91 (dd, *J* = 8.50, 1.0)	107.15	6.91 (dd, *J* = 8.53, 1.0)	107.46	7.05 (dd, *J* = 8.5, 0.8)	107.44	7.08 (d, *J* = 8.28)
9	157.53	-	157.29	-	156.82	-	156.64	-
10	110.76	-	111.01	-	110.05	-	110.04	-
5-OH	-	12.69, s	-	12.66, s	-	12.66, s	-	12.65, s
1′	111.04	-	117.18	-	109.01	-	115.02	-
2′	158.5	-	146.99	-	156.53	-	147.45	-
3′	103.93	6.65 (d, *J* = 8.53)	148.40	-	108.74	6.62 (dd, *J* = 8.3, 1.8)	145.15	-
4′	132.41	7.42 (t, *J* = 8.5)	115.49	7.03 (d, *J* = 9.03)	132.49	7.32 (t, *J* = 8.3)	117.22	7.12, (d, *J* = 9.03)
5′	103.93	6.65 (d, *J* = 8.53)	106.16	6.69 (d, *J* = 9.03)	102.23	6.62 (dd, *J* = 8.3, 1.8)	110.83	6.7, (d, *J* = 9.03)
6′	158.5	-	151.56	-	158.21	-	149.47	-
2′-OH	-	-	-	-	-	10.13, s	-	-
6′-OH	-	-	-	-	-	-	-	9.74, s
2′-OCH_3	55.98	3.81, s	61.48	3.88, s	-	-	60.94	3.77, s
3′-OCH_3	-	-	56.53	3.87, s	-	-	56.55	3.78, s
6′-OCH_3	55.98	3.81, s	56.17	3.77, s	55.95	3,75, s	-	-

A, B: the solvent used was $CDCl_3$ or DMS-d_6, respectively.

2.1.1. 1,3-Diphenylpropane-1,3-Dione (Dibenzoylmethane) (**1**)

After recrystallization, compound **1** was obtained in two polymorphic forms: pale-yellow-colored crystals in a monoclinic polymorph and large yellow-colored crystals in their orthorhombic form. Based on the ion 223.07645 *m/z* $[M-H]^-$ obtained using HRMS in the negative ionization mode, the molecular formula was established as $C_{15}H_{12}O_2$. Ultraviolet analysis allowed the registration of two absorption maxima at 252 and 345 nm. The comparison of the NMR spectra with the literature data [15] as well as the results from the crystallographic analysis [16] made it possible to confirm that the obtained compound was 1,3-diphenylpropane-1,3-dione, which was previously found to occur as a minor constituent of licorice [17]; *Acca sellowiana* essential oil [18]. This compound is often present as in equilibrium, having two tautomeric forms (see, Figure 1)

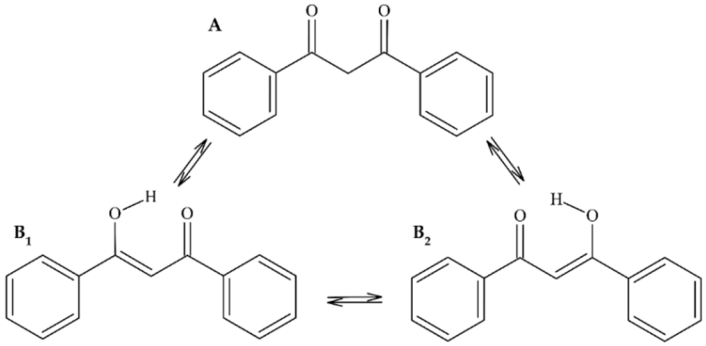

Figure 1. Chemical structure of compound **1.** The structures represent the tautomeric keto (**A**) and enol (**B_1**, **B_2**) forms in equilibrium.

2.1.2. 5-Hydroxyflavone (Primuletin) (**2**)

Compound **2** was obtained as yellow needle crystals. Based on the obtained parent ion 237.05572 $[M-H]^-$, the following molecular formula was generated: $C_{15}H_{10}O_3$. The recorded UV spectrum (271, 336 nm) made it possible to search for the compound structure among the flavones group. This hypothesis was confirmed by the bathochromic shift (42 nm) caused by the addition of sodium methoxide (NaOMe), which proved that there is no free -OH group at the C-3 carbon. On the other hand, the complex with aluminum chloride ($AlCl_3$), which is unstable in the presence of hydrochloric acid (HCl), confirmed the presence of the -OH group at C-5 (unstable bathochromic shift, 58 nm). The lack of a shift in the absorption maximum after the addition of sodium acetate ruled out the presence of a free -OH group at the C-7 carbon and ortho substitutions on the A and B rings after the impact of boric acid (H_3BO_3) [19]. The NMR spectra also provided fundamental information such as singlet δ_H 6.75, which corresponded to a proton on carbon atom C-3 and a value of δ_C 106.05, which is typical of flavone molecules. Moreover, the structure of isoflavone was excluded by C-2 chemical shifts at δ_C 164.55 [20,21]. The presence of the hydroxyl group at C-5 was certified by δ_H 12.58 (1H, s).

According to the information provided above as well as the results of the crystallographic analysis (see Table S1, Supplementary material), compound **2** was determined to be 5-hydroxyflavone (5-hydroxy-2-phenyl-4*H*-chromen-4-one), known as a primuletin, a natural product found in *Conchocarpus heterophyllus* [22], *Primula denticulate* [23], and *P. turkestanica* [24].

2.1.3. 5-Hydroxy-2′-Methoxyflavone (**3**)

The isolation process led to compound **3** being obtained as pale-yellow needle crystals. The recorded UV spectrum (271, 336 nm) allowed the compound to be classified into flavones. An analysis of the changes in the UV spectrum using ionizing and complexing reagents resulted in similar conclusions as those drawn in compound **2** [19]. Based on the 267.053 *m/z* $[M-H]^-$ ion peak, the molecular formula $C_{16}H_{12}O_4$ was generated. Moreover,

the apparent loss of 15 *m/z* [M-H-CH_3]$^-$ is indicative of the degradation of the methoxyl moiety. One-dimensional NMR spectra confirmed the methoxylation in ring B (δ_H 3.95, 1H, s; δ_C 55.67). To summarize the results obtained from the spectral and spectroscopic analyses as well as from the available scientific literature [25] and crystallographic data (see Table S1), compound **3** was determined to be 5-hydroxy-2′-methoxyflavone (5-hydroxy-2-(2-methoxyphenyl)-4*H*-chromen-4-one). Compound **3** has previously been found in *Iris ensata* [25].

2.1.4. 5-Hydroxy-2′,6′-Dimethoxyflavone (**4**)

Compound **4** was obtained as thin, white needle crystals. The registered predominant ion at 297.0772 *m/z* [M-H]$^-$ (see Figure S1) meant that the molecular formula was determined to be $C_{17}H_{14}O_5$, with an error in relation to the theoretical mass value of 1.35 ppm. Attempting to determine the structure by analyzing the changes in the UV spectrum allowed the compound to be classified as a flavone derivative (260, 327 nm) (see Figure S2) [19]. The analysis of the ^{1}H and ^{13}C NMR spectra in comparison to the previous structure revealed the lack of the proton signal at C-2′ and C-6′, with the simultaneous appearance of a characteristic signal for the methyl group (δ_H 3.81, 6H, s; δ_C 55.98) (see Figures S3 and S4 and Table 1). This allowed us to determine the symmetrical conformation of the B ring and its substitution with two methoxyl groups on C-2′ and C-6′, respectively.

Investigation of the homonuclear through-bond (COSY) and through-space (ROESY) correlations (see Figures S5 and S6) confirmed the hypothesis that there were two -CH_3 groups. Additionally, the protons attached to C-6-C-7-C-8 and C-3′-C-4′-C-5′, showed a direct relationship, and the ^{1}H-^{1}H interaction in that space attached to carbon atoms C-3′ and C- 5′ via the protons of the methyl moiety at the previously suggested site (C-2′ and C-6′). Finally, the connection of the information presented above with the correlations with the HMBC confirmed the dependence of the proton on the substituent via its correspondence with the correlating carbon (-CH_3 δ_H 3.81 and C-2′, C-6′ δ_C 158.51) (see Figure S7). The arguments presented above were also supported by HMQC and the X-ray diffraction results (see and Figure S8 and Table S1). A graphic representation of this dependency is presented in Figure 2. The available literature indicates the presence of a compound exemplifying a constitutional substitution isomer (5-hydroxy-6,2′-dimethoxyflavone) [26]. Furthermore, the symmetry of the B ring is shown to comprise equivalent atoms with the signals δ_H 3.81 (6H, s) and δ_C 55.98 as well as the signals corresponding to the HC-6 proton (δ_H 6.8 (1H, dd, *J* = 8.03, 0.75 Hz)). In conclusion, compound **4,** which is a new natural product, was determined to be 5-hydroxy-2′,6′-methoxyflavone (5-hydroxy-2-(2,6-dimethoxyphenyl)-4H-chromen-4-one).

2.1.5. 5-Hydroxy-2′,3′,6′-Trimethoxyflavone (**5**)

Compound **5** was crystallized as bright yellow cubes. The registered predominant ion 327.08874 [M-H]$^-$ meant that the molecular formula was determined to be $C_{18}H_{16}O_6$, with an error mass value of 1.36 ppm. The obtained UV spectrum (257, 331 nm) suggested that the substance was a flavone (see Figure S9). Moreover, the results show a bathochromic shift of the I band comprising compounds **2**–**4**, resulting in the prospective increase in the oxygenation of the B-ring. On the other hand, the oxygenation pattern of the B-ring does not cause a shift in band II [19] in the MS spectrum ions (313, 297, 282 *m/z*), indicating the loss of the [M-H-CH_3]$^-$ fragment connected to the presence of three methoxy groups (see Figure S10). This assumption was confirmed by one-dimensional NMR spectra. Additionally, two doublets at δ_H 7.03 and δ_H 6.69 with the coupling constant *J* = 9.03 Hz indicated a connection between C-4′ and C-5′ with no protons in the vicinity. They submitted the asymmetric distribution of the substituents on the B ring (see Figures S11 and S12 and Table 1). The ^{1}H-^{1}H correlation only revealed proton interactions at carbon atoms C-4′ and C-5′ in ring B. Ring A, beyond the OH group at C-5, showed no substitution (see Figure S13). The spatial proximity of the methyl groups was also indicated by the strong NOE interaction of the protons of these groups when they were substituted for

carbon atoms C-3 'and C-6′ (see Figure S14). A detailed analysis of the data from the HSQC correlation allowed the protons directly belonging to the methyl group to be determined (δ_H 3.88, δ_C 61.48; δ_H 3.87, δ_C 56.53; and δ_H 3.77, δ_H 56.17 for substitutions at C-2′, C-3′, and C-6′, respectively) (see Figure S15). On the other hand, the analysis of the HMBC spectrum allowed the coupling between the protons of the methyl groups and the carbon atoms in the B ring to be determined (δ_H 3.88, δ_C 146.99; δ_H 3.87, δ_C 148.40; and δ_H 3.77, δ_C 151.56 for substitutions at C-2′, C-3′, and C-6′, respectively) (see Figure S16). To summarize, using the results and data obtained from the crystallographic analyses (see Table S1), compound **5,** a new natural product, was determined to be 5-hydroxy-2′,3′,6′-methoxyflavone (5-hydroxy-2-(2,3,6-trimethoxyphenyl)-4*H*-chromen-4-one).

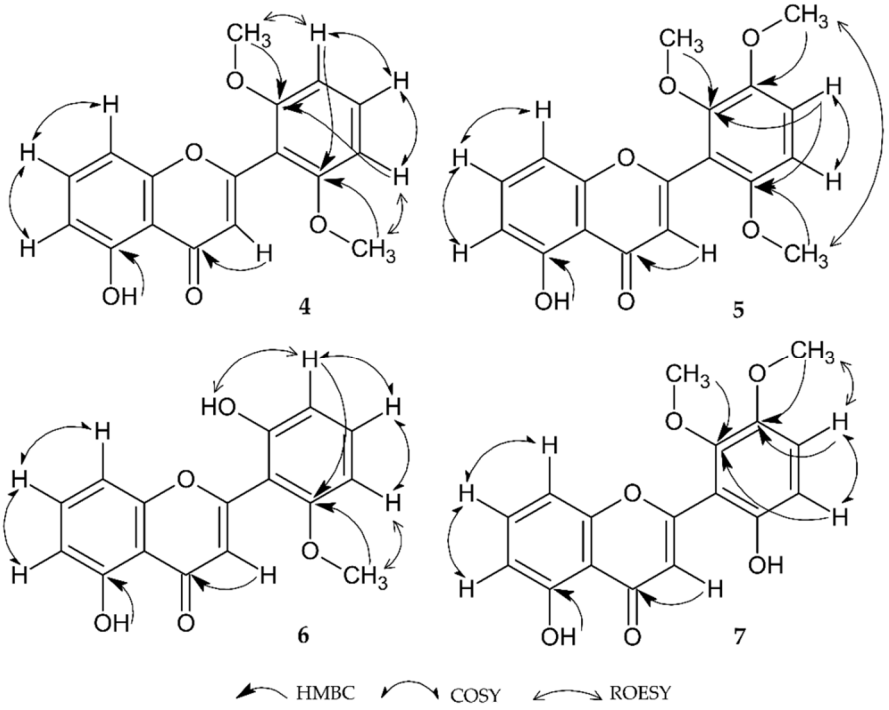

Figure 2. Essential correlation for the structural elucidation of compounds **4**–**7**.

2.1.6. 2′,5-Dihydroxy-6-Methoxyflavone (**6**)

Compound **6** was obtained as thin white needle crystals. The obtained predominant ion 283.06166 $[M-H]^-$ meant that the molecular formula was determined to be C_{16} H_{12} O_5, with an error mass value at 1.65 ppm (see. Figure S17). The obtained UV spectrum (259, 327 nm), as in the case of compounds **2–5**, confirmed that the isolated compound was a flavone with an -OH group at C-5 carbon (unstable bathochromic shift 58 nm, after $AlCl_3$ addition) and a high degree of B-ring oxidation (band I = 327 nm) (see Figure S18) [19]. The ^{1}H NMR analysis showed an additional -OH group (δ 10.13, 1H, s), one methyl group (δ 3.75, 3H, s) and no A and C ring substituents. Two triplets at δ_H 7.65 (J = 8.3 Hz) and δ_H 7.32 (J = 8.3 Hz) from C-7 and C-4′, respectively, indicated the proximity of other protons (see Figure S19 and S20 and Table 1). Their direct connections were confirmed by the COSY correlation (see Figure S21). Moreover, using the HMQC correlation, all the protons that were directly bound to carbon were correlated (see Figure S22). Then, the determination of the methyl vincinal proton's interaction with carbon atom (δ_H 3.75, δ_C 158.21) and the geminal interaction of the proton of both OH groups (δ_H 10.13, δ_C 156.53; δ_H 12.69, δ_C 159.95; C-2′ and C-5, respectively) allowed the final configuration to be determined (see Figures S22 and S23). The data presented above were also supported by the X-ray diffraction results (see Table S1) and the ROESY correlation analysis (see Figure S24). The collected results allowed for compound **6** to be recognized as 2′, 5-dihydroxy-6-

methoxyflavone (5-hydroxy-2-(2-hydroxy-6-methoxyphenyl)-4*H*-chromen-4-one), another new structure being described for the first time in plants.

2.1.7. 5,6′-Dihydroxy-2′,3′-Dimethoxyflavone (**7**)

Compound **7** was also obtained in the form of thin white needle crystals during the recrystallization process. The molecular ion 313.07244 $[M-H]^-$ meant that the molecular formula was determined to be $C_{17}H_{14}O_6$, with an error in relation to the theoretical value at 2.4 ppm (see Figure S25). The UV spectrum indicated that it was a flavone derivative (258, 333 nm). The value of band I in the spectrum indicated a high degree of B ring oxidation (see Figure S26). Additionally, in the mass spectrum, a 2-fold loss of 15 *m/z* relative to the parent ion suggests the cleavage of the 2 methoxy groups. Moreover, the presence of a 255 *m/z* ion that is typical of dihydroxyflavone formed via the complete degradation of the CH_3 groups (see Figure S25). Further, the ^1H spectrum showed signals from two asymmetrically arranged methyl groups (δ 3.77, 3H, *s*; δ 3.78, 3H, *s*), and an -OH group (δ 9.74, 1H, *s*) allowed locating them in the B ring as opposed to in the -OH group (δ 12.65, 1H, *s*) attached to C-5 (see Figure S27 and S28 and Table 1). A detailed analysis of the correlation spectra provided specification of the structure configuration. COSY analysis confirmed the lack of A ring substitution. More importantly, it proved that correlation could only be observed between the protons at the HC-4′ and HC-5′ carbons (see Figure S29). On the other hand, ROESY confirmed proton interaction in the methyl attached at C-3′ and the proton at HC-4′, while HMBC analysis confirmed the location of both methyls (δ_H 3.77, δ_C 147.45; δ_H 3.78, δ_C 145.15, C-2′ and C-3′, respectively) (see Figures S30 and S31). Taking the above results, HSQC analysis (see Figure S32) and the crystallographic analysis data into consideration (see Table S1), we concluded that compound **7** is a new structure of natural origin called 5, 6′-dihydroxy-2′,3′-dimethoxyflavone (5-hydroxy-2-(6-hydroxy-2,3-dimethoxyphenyl)-4*H*-chromen-4-one). The structures of the analyzed substances are shown in Figure 3.

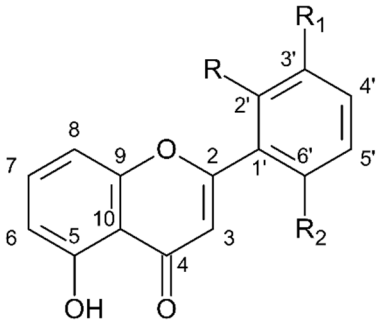

Compound	R	R_1	R_2
2	-H	-H	-H
3	$-OCH_3$	-H	-H
4	$-OCH_3$	-H	$-OCH_3$
5	$-OCH_3$	$-OCH_3$	$-OCH_3$
6	-OH	-H	$-OCH_3$
7	$-OCH_3$	$-OCH_3$	-OH

Figure 3. Chemical structures of compounds **2–7**.

2.2. Quantification of Flavones (1–7) in Selected Extracts

The secondary metabolites obtained from the flavonoid group were quantified using a liquid chromatograph equipped with a photodiode array detector (HPLC-PDA). The applied C8 column allowed for the reduction of the organic mobile phase modifier used during the analysis as well as the reduction of the retention time of the compounds, which

made the method environmentally friendly and cost-effective. In the selected extracts (**HP1**, **HP6–8**), the content of isolated compounds (**1–7**) as well as the zapotin (**ZAP**) found in the raw material in previous analyses [11,25] was determined (see Table 2 and Figures S33 and S34). The highest content was found in **HP6** (338 μg/mg), followed by **HP7** (76.31 μg/mg). The lowest flavonoid content was determined in **HP8** (7.99 μg/mg). Such a dependence confirms the legitimacy of isolation from the **HP6** extract and proves that the isolated non-polar compounds will go to the extracts from the initial phase of extraction, remaining almost completely extracted from the plant material.

Table 2. Quantification results of the flavonoids in the extracts **HP1** and **HP6–8**.

Compounds	Content of Compounds Expressed as μg/mg of Dry Extract			
	HP1[A]	**HP6**[A]	**HP7**[A]	**HP8**[A]
1	0.81 ± 0.01	2.7 ± 0.01	4.98 ± 0.01	0.26 ± 0.01
2	0.29 ± 0.01	10.04 ± 0.02	1.76 ± 0.01	0.22 ± 0.01
3	1.31 ± 0.01	58.82 ± 0.44	6.02 ± 0.03	0.86 ± 0.01
4	1.05 ± 0.01	39.19 ± 0.09	8.44 ± 0.05	0.75 ± 0.01
5	0.67 ± 0.01	29.57 ± 0.02	5.34 ± 0.02	0.51 ± 0.01
6	0.9 ± 0.01	24.84 ± 0.15	10.21 ± 0.03	0.9 ± 0.01
7	1.26 ± 0.01	18.76 ± 0.36	7.83 ± 0.07	0.66 ± 0.01
ZAP	8.13 ± 0.06	154.77 ± 0.19	31.73 ± 0.13	3.84 ± 0.04
Sum	14.42 ± 0.01	338.68 ± 0.16	76.31 ± 0.04	7.99 ± 0.01

A: the content expressed as mean with standard deviation.

Moreover, **ZAP** (3.84–154.77 μg/mg) was dominant in all fractions, followed by compound **3** (0.86–58.82 μg/mg) in **HP1**, **HP6,** and **HP8** and compound **6** (10.21 μg/mg) in **HP7**.

2.3. Cell Viability

An MTT assay for each sample was performed for a preliminary estimation of the cytotoxic effects of the extracts **HP1** and **HP6**–**HP8** (6.25–200 μg/mL), compounds **1–7** and **ZAP (**6.25–200 μM) in human tongue squamous carcinoma cells SCC-25 and normal fibroblasts after 24 h and 48 h of incubation (see Table 3). The ability of the tested samples to induce cytotoxic effects in SCC-25 cells was only observed for the selected compounds. It is worth mentioning that there are several reports with information on the reducing effect of plant metabolites on the conversion of tetrazolium dye to formazan. However, the reduction is connected to the presence of a catechol group as well as free OH groups at C-3 and C-5′ [27,28]. The examined compounds do not have groups that can disturb the reliability of the measurements.

The MTT study showed that SCC-25 cell viability was inversely proportional to the applied concentration of all of the tested compounds. The cytotoxic potential is expressed as a median inhibitory concentration (IC_{50}) value, where the studied extracts and compounds inhibited the viability of the SCC-25 cells in a dose-dependent manner. The highest activity was observed after treatment with compounds **1** and **7** as well as with **ZAP** after both 24 h and 48 h of incubation (see Table 3). The IC_{50} values of the other compounds were >200 μM (highest tested concentration). The IC_{50} values after 48 h of incubation for some extracts were worth emphasizing (HP6, IC_{50} = 14.9 μg/mL; HP7, IC_{50} = 16.7 μg/mL) as they reached half of the effectiveness cisplatin, which was used as a positive control (**cPT**, IC_{50} = 7.58 μg/mL). It is worth noting that the activity of all of the tested samples was higher after 48 h of incubation than after 24 h. Moreover, it can be assumed that the cytotoxic effect of the extracts correlates with the content of all of the flavones present (**HP6** > **HP7** > **HP1** > **HP8**) as well as the **ZAP** and compound **7** content. The viability of the fibroblast under the influence of **HP1** and **HP6** and **1**, **7**, and **ZAP** was significantly higher than it was in the SCC-25 cells (above 200), and for **HP7** it was 58.9 ± 2.94 μg/mL.

Table 3. IC_{50} of viability of SCC-25 human tongue squamous and fibroblast cells treated for 24 h and 48 h with different concentrations of the extracts **HP1** and **HP6**-**HP8** and compounds **1–7** isolated from *H. palustris* and zapotin (**ZAP**).

	24 h		48 h	
Sample	**SCC-25**	**Fibroblasts**	**SCC-25**	**Fibroblasts**
HP1 [A]	37.3 ± 1.86	>200	30.3 ± 1.15	>200
HP6 [A]	50.88 ± 2.54	>200	14.9 ± 0.74	>200
HP7 [A]	48.4 ± 2.40	>200	16.7 ± 0.83	58.90 ± 2.94
HP8 [A]	>200	-	>200	-
1 [B]	39.98 ± 1.89	>200	29.1 ± 1.45	>200
2 [B]	>200	-	>200	-
3 [B]	>200	-	>200	-
4 [B]	>200	-	>200	-
5 [B]	>200	-	>200	-
6 [B]	>200	-	>200	-
7 [B]	78.2 ± 3.25	>200	40.6 ± 1.65	>200
ZAP [B]	64.94 ± 3.24	>200	20.33 ± 1.01	>200
cPT [B,C]	26.1 ± 1.03	>200	7.58 ± 0.37	40.50 ± 2.01

A: expressed as μg/mL; B: expressed as μM; all values are represented as the mean ± standard deviation (SD) from at least three independent repeats; C: **cPT**-cisplatin as a positive control.

The morphological profile of SCC-25 squamous carcinoma cells after 24 h and 48 h of incubation with **HP1**, **HP6** and **HP7** at the concentration of 100 μg/mL, and **1**, **7**, **ZAP**, and **cPT** are shown in Figures 4 and 5. We observed slope in cell adhesion and decreased the number of cells in the treatment groups compared to the untreated group, displaying the inhibition of cell proliferation.

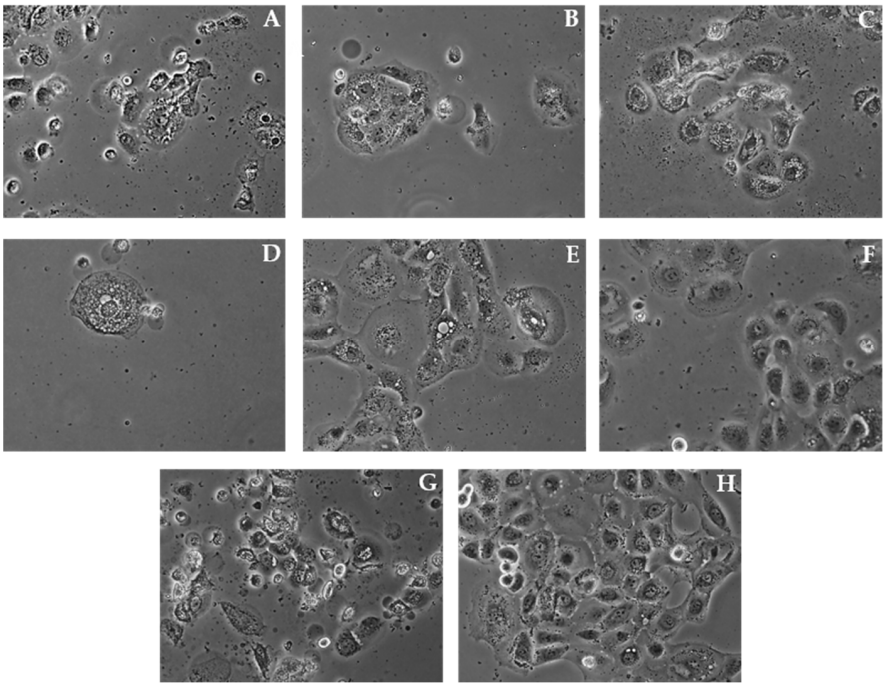

Figure 4. Morphological profile of SCC-25 cells after 24 h of incubation with **HP1** (**A**), **HP6** (**B**), and **HP7** (**C**) at the concentration of 100 μg/mL and with **1** (**D**), **7** (**E**), **ZAP** (**F**), and **cPT** (**G**) at 100 μM concentrations compared the untreated control cells (**H**).

In order to determine the potential mechanism of action, the level of the pro-apoptotic proteins was determined via the Western blot method. The obtained results did not indicate the presence of this kind of activity (unpublished data). It is confirmed by micropho-

tographs (Figures 4 and 5) that show no typical morphological features of apoptosis, in particular cell membrane blebbing and formation of apoptotic bodies. Considering this fact, an evaluation determining whether the cytotoxicity of the samples was the result of their influence on the biosynthesis of cell DNA was carried out by assessing the capability of intracellular thymidine incorporation. A downregulation in the DNA biosynthesis in the SCC-25 cells was observed for all the tested samples (see Figures 6 and 7).

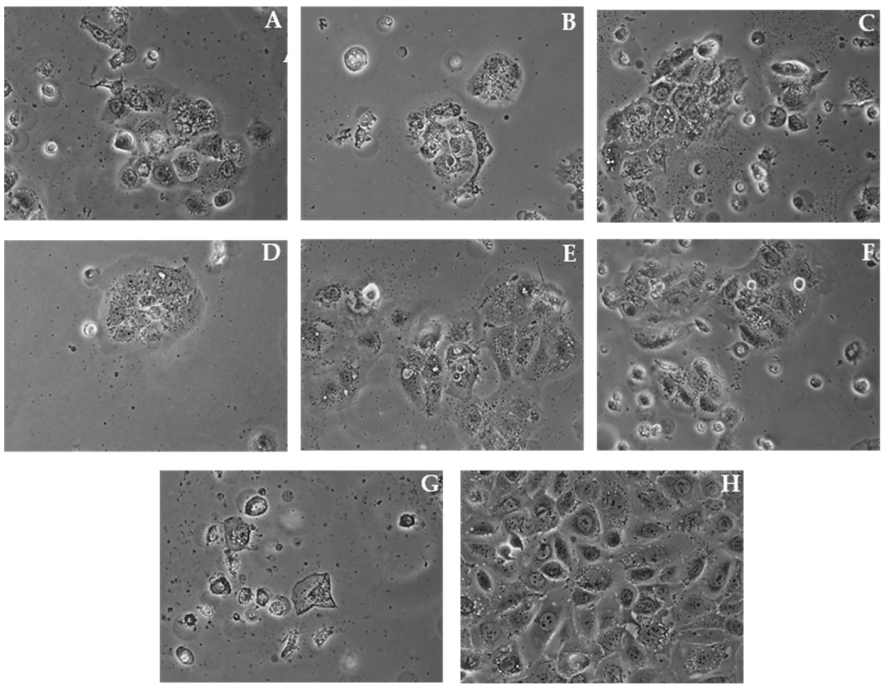

Figure 5. Morphological profile of SCC-25 cells after 48 h of incubation with **HP1** (**A**), **HP6** (**B**), and **HP7** (**C**) at the concentration of 100 µg/mL and with **1** (**D**), **7** (**E**), **ZAP** (**F**), and **cPT** (**G**) at 100 µM concentrations compared to the untreated control cells (**H**).

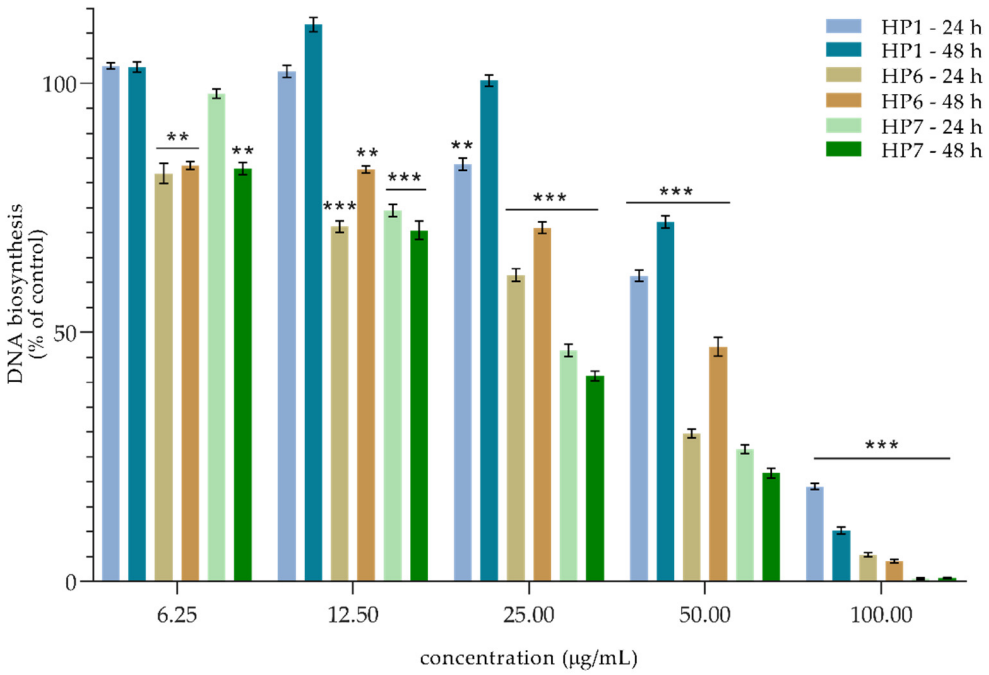

Figure 6. The decreasing effects of **HP1**, **HP6**, and **HP7** extracts (µg/mL) on DNA biosynthesis in SCC-25 cells after 24 h and 48 h of incubation. Mean percentage from at least three independent experiments carried out in duplicate are presented. ** $p < 0.01$ versus control group, *** $p < 0.001$ versus control group.

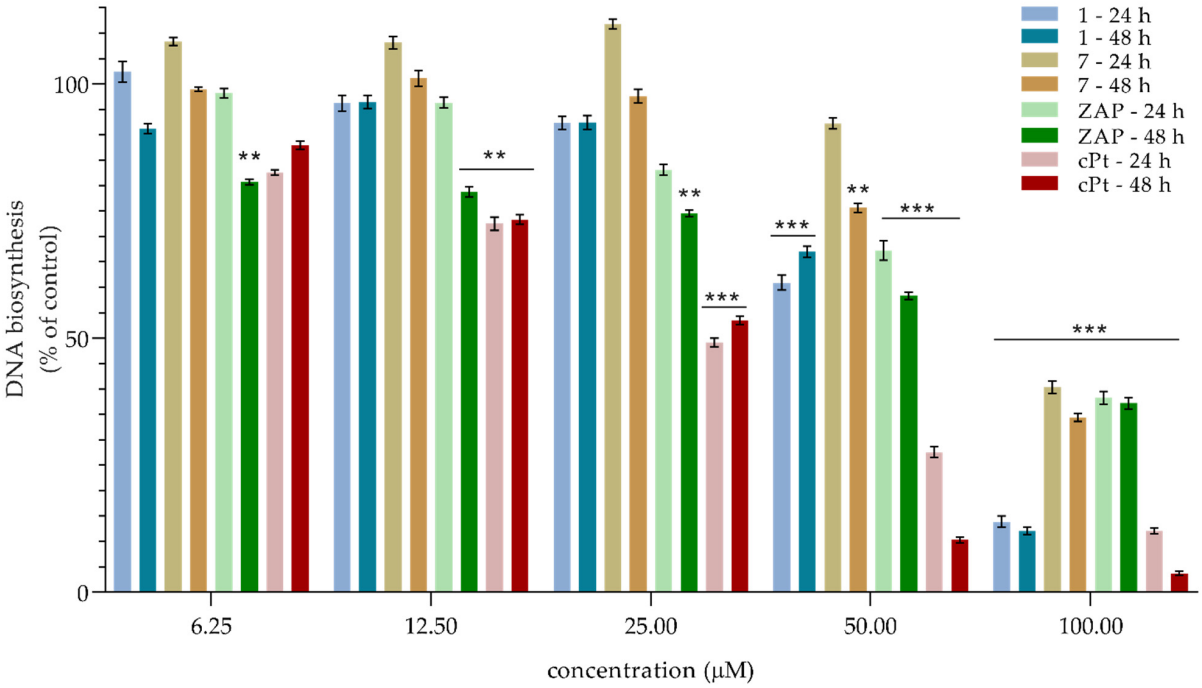

Figure 7. The decreasing effects of **1**, **7**, zapotin (**ZAP**), and **cPT** (μM) on DNA biosynthesis in SCC-25 cells for 24 h and 48 h of incubation. Mean percentages from at least three independent experiments conducted in duplicate are presented. ** $p < 0.01$ versus control group, *** $p < 0.001$ versus control group.

Relating these effects to the isolated compounds, dose-dependency appears at concentrations above 25 μM. Most importantly, the potency of **ZAP** after 48 h shows an effect similar to that of the positive control, **cPT**. The assessed cytotoxic effect and the influence on DNA synthesis may suggest that the mechanism of action in the samples is based on the influence on cell division via an arrest of the division in the S phase of the cell cycle. Our results revealed that the viability of cancer cells is the most strongly affected by **ZAP** compared to any of the other flavonoids isolated from *H. palustris*. Zapotin (**ZAP**), which has been tested on numerous biological models, including on the human bladder carcinoma cell (T24), human liver cancer cell (HepG2), and human leukemia cell (HL-60) lines, showed suppression in the G2/M phase of the cycle [29]. In addition, the current reports on the polymethoxyflavones confirm the cystostic mechanism of action consisting in arrest of the cell cycle [30]. Although the effect on different lines cannot be directly correlated, compound **1**, identified as dibenzoylmethane, has already shown cell-cycle deregulation in melanoma cells [31]. In light of the available literature and the results obtained, flavonoids show the strongest multidirectional action for use as anticancer agents [32].

To the best of our knowledge, the results presented above are the first detailed report comparing nonpolar extracts or compounds from *H. palustris* and describing their activity on the oral squamous carcinoma cell line (SCC-25). The obtained structures bring new light to the derivatives of secondary metabolites from the polymethoxyflavones group and extend to possible directions for compound biosynthesis in plant tissues. Moreover, it seems correct to suppose that the chemotaxonomic markers present in the Primulaceae family species, such as primuletin [21,22], can be extended with another potential chemophenetic factor such as zapotin [31].

3. Materials and Methods

3.1. Chemicals and General Methods

Petroleum, *n*-hexane, chloroform, and methanol were purchased from Avantor (Gliwice, Poland). Sephadex LH_{20} was purchased from GE Healthcare (Uppsala, Sweden). The

adsorbent used for LPLC, silica gel 60 (0.063–0.2 mm), and a TLC aluminum plate coated with silica gel 60 F_{254} were purchased from Merck (Darmstadt, Germany). Formic acid was purchased from Sigma Aldrich Co. (St. Louis, MO, USA). Tetrahydrofuran HPLC grade was purchased from Honeywell (Seelze, Germany). Acetonitrile Optima (LC/MS grade) was purchased from Fisher Scientific (Loughborough, UK). Ultrapure water was obtained using the POLWATER DL3-100 system (Kraków, Poland). The cell viability and proliferation assays were performed on the human tongue squamous cell line (SCC-25). The cells were obtained from ATCC (CRL-1628, American Type Culture Collection, Manassas, VA, USA) and cultured in a 1:1 mixture of DMEM (Dulbecco's minimal essential medium) and Ham's F12 medium (Thermo Fisher Scientific, Waltham, MA, USA, 31330038) supplemented with 400 ng/mL hydrocortisone (Sigma-Aldrich, Burlington, MA, USA, H0135), 10% FBS (fetal bovine serum, Thermo Fisher Scientific, Waltham, MA, USA, 10270106), and penicillin–streptomycin solution (Thermo Fisher Scientific, Waltham, MA, USA, 15140122). Furthermore, for the cytotoxicity assay, human skin fibroblasts (CCD25Sk) cultured in DMEM (Thermo Fisher Scientific, Waltham, MA, USA, 41966029) supplemented with 10% FBS and penicillin-streptomycin solution were used. The cells were incubated at 37 °C in the air with 5% CO_2. PBS (14190136) was purchased from Thermo Fisher Scientific (Waltham, MA, USA,). MTT (M5655), SDS (L3771), and cisplatin (cPT), which was used as a positive control (P4394), were purchased from Sigma-Aldrich (Burlington, MA, USA). Zapotin was purchased from Biosynth-Carbosynth (Compton, UK). The [^{3}H]-thymidine (#MT6037) for the proliferation assay was obtained from Hartmann Analytic (Braunschweig, Germany). Extract preparation was carried out using an ultrasonic bath (40 kHz, Sonic-5, Polsonic, Warsaw, Poland). Solvent residues were removed by distillation (Rotavapor R-215 coupled with vacuum controller V-855 (Büchi, Flawil, Switzerland) and freeze-drying (Lymph-lock, Labconco, Kansas City, MO, USA). The HPLC–PDA analyses were performed using an Agilent Infinity apparatus equipped with a 1260 high pressure binary pump, a 1260 ALS sampler, a 1260 TCC column oven, and a 1290 photodiode array detector (Agilent Technologies, Santa Clara, CA, USA). UV spectra were measured with an Analytic Jena SPECORD 200 Plus instrument (Jena, Germany). Melting points were obtained using a BÜCHI 535. NMR spectra were recorded on a Thermo Fisher Scientific Bruker Avance II 400 spectrometer (Billerica, MA, USA). High-resolution mass spectra were recorded using a 6230 TOF mass spectrometer (Agilent Technologies, Santa Clara, CA, USA). Specific rotation [α] was recorded using a P-2000 digital polarimeter (Jasco, Hachioji, Tokyo, Japan) at 25 $\pm$ 0.5 °C and at the sodium D line.

3.2. Plant Material

Hottonia palustris herb (HP) was collected at the turn of April and May 2019 before flowering from a wild habitat in the wetlands of the Puszcza Knyszyńska (53°17′13.2″ N, 22°53′42.0″ E). Taxonomic identification was carried out based on the scientific botanical literature [33]. A voucher specimen (No. HP-17040) was deposited in the Herbarium of the Department of Pharmacognosy Medical University of Białystok, Poland.

3.3. Preparation of the Extracts

Immediately after harvesting, the plant material was dried under shade and air ventilation at ambient temperature (1100 g). The ultrasound-assisted extraction technique was used to obtain the crude methanol extract **HP1**. Milled and accurately weighed plant material (15 g) was extracted five times at 40 $\pm$ 2 °C with 0.05 L of methanol. Subsequently, the extract was centrifuged, filtered, concentrated under the vacuum at 40 $\pm$ 2 °C, and lyophilized. The continuous extraction technique in the Soxhlet apparatus was used to prepare the lipophilic extracts. Milled and accurately weighed HP herb (1160 g) was exhaustively extracted with petroleum. The solvent was removed under a vacuum at a controlled temperature (40 $\pm$ 2 °C) to produce a crude extract (**HP6**, 1.5 L $\times$ 45, yield 75 g). After the solvent was evaporated, the plant material was etched with chloroform. Then, the solvent was removed under a vacuum at a controlled temperature (40 $\pm$ 2 °C)

to produce a crude extract (**HP7**, 1.5 L × 30, yield 28 g). Then, the purified plant material was subjected to exhaustive extraction with methanol under reflux. Afterwards, the lipid compounds were discarded, and the plant sample was subjected to exhaustive extraction with methanol and then with 50% methanol solution (4.5 L × 20, each). Subsequently, the combined methanol extracts were evaporated from the solvent at a lowered pressure, dissolved in water, and partitioned into the chloroform phase (**HP8**, 0.1 L × 45). The water residue was lyophilized and intended for further research. Each time, the efficiency of the extraction process was controlled using thin-layer chromatography. All of the extracts were suspended in water, frozen and lyophilized.

3.4. Isolation Procedures

The low-pressure liquid chromatography (LPLC) technique was used as a preliminary isolation step. After conditioning, the elution was carried out on a Sephadex LH_{20} column in an isocratic with a mixture of chloroform and methanol (3:2, *v*/*v*). The 18 fractions were collected. After verification via the TLC technique (silica gel, solvents *n*-hexane: ethyl acetate (8:2, *v*/*v*)) and combination, five fractions were finally obtained. Then, a fourth, flavonoid-rich fraction was separated on an LPLC column packed with silica gel. Elution was performed with an *n*-hexane and ethyl acetate mixture with gradually increasing polarity. The 100 fractions were collected. After TLC analysis (silica gel plate, solvents *n*-hexane: ethyl acetate (8:2, *v*/*v*)), similar fractions were pooled. Finally, 21 fractions were obtained. As the solvent was allowed to evaporate under low pressure at room temperature, the compounds crystallized. Thus, compound **1** (425 mg), thereupon compound **2** (89 mg), was eluted one by one with *n*-hexane: ethyl acetate at a ratio of 95:5 (*v*/*v*). Then, compound **1** required recrystallization in pure hexane [16]. Compound **3** (729 mg) and compound **4** (480 mg) crystallized from the fraction and were eluted one by one at a ratio of 8:2 (*v*/*v*). Compounds **6** (130 mg) and **7** (white thin needle, 170 mg) were eluted one by one at a ratio of 7:3 (*v*/*v*). The dry residue of the fractions was recrystallized in a mixture of dichloromethane: ethanol (9:1, *v*/*v*). Thereafter, a residue was obtained from the fraction collected at a ratio of 6:4 (*v*/*v*), which was dissolved with a mixture of hot ethanol: water (98:2, *v*/*v*). As the solution gradually cooled, compound **5** (110 mg) crystallized.

3.5. Crystallographic Analysis

Crystals of compounds **2–7** were mounted on a loop with paraffine oil. The X-ray diffraction data were measured using Cu Kα radiation at 100 K on a SuperNova diffractometer (Rigaku, Akishima-shi, Tokyo, Japan) equipped with either a CCD detector (**2**–**4**) or XtaLAB Synergy (Rigaku, Akishima-shi, Tokyo, Japan) with a Hybrid Pixel two-dimensional detector HyPix-6000HE (**5**–**7**). All of the data were integrated and scaled using the CrysAlisPro software package (Rigaku, Akishima-shi, Tokyo, Japan). The crystal structures were determined using direct methods according to the OLEX2 [34] graphical interface with SHELXT [35] and were refined with SHELXL [36]. All of the non-hydrogen atoms were refined anisotropically using the full-matrix least-squares method. All of the hydrogen atoms were initially located on electron-density difference maps. The aromatic hydrogen atoms were constrained to idealized positions with C-H = 0.95 Å and $U_{iso}(H) = 1.2U_{eq}(C)$, whereas the methyl hydrogen atoms were constrained with C-H = 0.98 Å and $U_{iso}(H) = 1.5U_{eq}(C)$. The hydroxyl hydrogen atoms were freely refined. PLATON software [37] was used to validate the final crystallographic data. The CCDC entries: 2143620 (**2**), 2143614 (**3**), 2143617 (**4**), 2143615 (**5**), 2143619 (**6**), and 216092 (**7**), and contain the supplementary crystallographic data for this publication. These data can be obtained free of charge from The Cambridge Crystallographic Data Center, see [38]. The final data sets and refinement statistics for all of the crystal structures are reported in the Supplementary Materials in Table S1.

3.6. Compound Identification

1,3-diphenylpropane-1,3-dione (**1**): pale-yellow crystals, UV λ_{max} nm: 252, 345; +NaOMe: 240, 351; +$AlCl_3$: 267, 364; +NaOAc: 251, 344; +H_3BO_3: 252, 343. HRMS *m*/*z* = 223.07645

$[M-H]^-$ (calculated for $C_{15}H_{12}O_2$), difference = 3.2 ppm. Purity 98% by HPLC. For X-ray diffraction data, see [16]. For NMR spectral data, see [15].

5-hydroxyflavone (**2**): yellow needle, UV λ_{max} nm: 271, 336; +NaOMe: 276, 383; +$AlCl_3$: 293, 397; +NaOAc: 270, 336; +H_3BO_3: 271, 336. HRMS *m/z* = 237.05572 $[M-H]^-$ (calculated for $C_{15}H_{10}O_3$), difference = 5.52 ppm. Purity 98% by HPLC. X-ray diffraction data have been provided in Table S1. For NMR spectral data, see [21].

5-hydroxy-2′-methoxyflavone (**3**): pale-yellow needle crystals, UV λ_{max} nm: 260, 327; +NaOMe: 264, 371; +$AlCl_3$: 267, 388; +NaOAc: 261, 327; +H_3BO_3: 260, 336. HRMS *m/z* = 267.06753 $[M-H]^-$ (calculated for $C_{16}H_{12}O_4$), difference = 2.2 ppm. Purity 98% by HPLC. X-ray diffraction data have been provided in Table S1. For NMR spectral data, see [25].

5-hydroxy-2′,6′-dimethoxyflavone (**4**): white thin needle, (mp.: 173 °C); $[\alpha]_D$: -1.47 (DMSO; c = 0.1); UV λ_{max} nm: 260, 327; +NaOMe: 264, 371; +$AlCl_3$: 267, 388; +NaOAc: 261, 327; +H_3BO_3: 260, 336 (see Figure S2). HRMS *m/z* = 297.0772 $[M-H]^-$ (calculated for $C_{17}H_{14}O_5$), difference = 1.35 ppm (see Figure S1). Purity 98% by HPLC. X-Ray diffraction data have been provided in Table S1. For NMR spectral data, see Table 1 and Figures S3–S8.

5-hydroxy-2′,3′,6′-trimethoxyflavone (**5**): bright yellow cubes (mp.: 173 °C); $[\alpha]_D$: 0.56 (DMSO; c = 0.1); UV λ_{max} nm: 257, 331; +NaOMe: 267, 372; +$AlCl_3$: 268, 387; +NaOAc: 258, 331; +H_3BO_3: 257, 331 (see Figure S9). HRMS *m/z* = 327.08874 $[M-H]^-$ (calculated for $C_{18}H_{16}O_6$), difference = 1.36 ppm (see Figure S10). Purity 98% by HPLC. X-ray diffraction data have been provided in Table S1. For NMR spectral data, see Table 1 and Figures S11–S16.

2′, 5-dihydroxy-6-methoxyflavone (**6**): white thin needle, (mp.: 238 °C); $[\alpha]_D$: -0.21 (DMSO; c = 0.1); UV λ_{max} nm: 259, 327; +NaOMe: 268, 365; +$AlCl_3$: 267, 385; +NaOAc: 258, 327; +H_3BO_3: 259, 364 (see Figure S18); HRMS *m/z* = 283.06166 $[M-H]^-$ (calculated for $C_{16}H_{12}O_5$), difference = 1.65 ppm (see Figure S17). Purity 98% by HPLC. X-ray diffraction data have been provided in Table S1. For NMR spectral data, see Table 1 and Figures S19–S24.

5, 6′-dihydroxy-2′,3′-dimethoxyflavone (**7**): white thin needle, (mp.: 200 °C); $[\alpha]_D$: -0.21 (DMSO; c = 0.1); UV λ_{max} nm: 258, 333; +NaOMe: 243, 369; +$AlCl_3$: 268, 387; +NaOAc: 258, 332; +H_3BO_3: 257, 333 (see Figure S26); HRMS *m/z* = 313.07244 $[M-H]^-$ (calculated for $C_{17}H_{14}O_6$), difference = 2.4 ppm (see Figure S25). Purity 98% by HPLC. X-Ray diffraction data have been provided in Table S1. For NMR spectral data, see Table 1 and Figures S27–S32.

3.7. Method Development and Flavonoid Quantification in H. palustris by HPLC-PDA

The chromatographic method developed here was validated according to the guidelines outlined by the International Conference on Harmonisation (ICH) [39]. The parameters are summarized in Table S2 of the Supplementary Materials.

3.7.1. Standard Preparation

Accurately weighed 1 mg of compounds **1**–**7** and ZAP was dissolved in 1 mL DMSO and filtered through a 0.2 µm PVDF syringe filter into HPLC vials. Then, standard solutions were used to prepare the stock solution. In the next step, five-step mixtures were prepared using the multiple dilution method for the calibration curve. Measurements were started immediately after the solutions were prepared.

3.7.2. Sample Preparation

Accurately weighted extract samples were dissolved in DMSO. Then, they were diluted with the initial mobile phase to 10 mg/mL (*m*/*v*) (**HP1**), 1 mg/mL (*m*/*v*) (**HP6**), 5 mg/mL (*m*/*v*) (**HP7**), and 20 mg/mL (*m*/*v*) (**HP8**) and filtered through a 0.2 µm PVDF syringe filter into HPLC vials.

3.7.3. Analysis Conditions

The HPLC analyses were carried out on a reverse phase Kinetex XB-C8 column (batch No.: 5606-0137, 150 × 2.1 mm, 1.7 µm; Phenomenex, Torrance, CA, USA) and were protected by the precolumn. Mobile phase A was a mixture of 2% formic acid in water and tetrahydrofuran (8:2, *v*/*v*), and mobile phase B was a mixture of 2% formic acid in acetonitrile and tetrahydrofuran (8:2, *v*/*v*). A three-step gradient solvent system, 0–3 min, 20% B; 3–30 min, 20–37% B; and 30–35 min, 37% B, was used with 10 min equilibration. The flow rate was 150 µL/min. The column was thermostated at 25 ± 0.5 °C. The volume of the injected samples was 1 µL. UV-Vis spectra were recorded over a range of 190–600 nm, and chromatograms were acquired at 258 nm (**ZAP**, compounds **4**–**7**), 270 nm (compounds **2**, **3**), and 345 nm (compound **1**) wavelengths, which matched the value of the most intense absorption peak. For every tested compound, the calibration curve was obtained by plotting the peak areas versus the number of standards. The contents of the compounds in the samples were calculated using the regression parameters of the calibration curves.

3.7.4. Specificity, Linearity and Range

Specificity was tested by comparing the retention times, peaks purity, and UV spectra of the compounds in the extracts with standards. The analysis of the obtained UV chromatograms made it possible to exclude the possibility of co-elution (see Figures S33 and S34). To evidence a linear relationship between the compound signals and the compound concentration, determinations were performed for five concentrations in triplicate. The working range was defined by the restrictive limit of quantification and the highest concentration allowing for linearity.

3.7.5. Accuracy

Accuracy was assessed by testing the recovery. The ratio of the known added concentration of standard compound to the concentration of standard compound calculated based on the calibration curve developed with the HPLC-PDA method was determined and expressed as a percentage of recovery.

3.7.6. Precision

Precision was assessed by testing the repeatability of six independent sample solutions (intraday) and by carrying out intermediate precision analysis on three independent sample solutions on different days (interday).

3.7.7. Limit of Detection (LOD) and Limit of Quantification (LOQ)

According to the guidelines outlined by the ICH [39], we have adopted the standard deviation value of the intercept (σ) divided by the slope (s) of the calibration curves multiplied by 3.3 and have then multiplied for limit of detection (LOD) and multiplied by 10 to determine the limit of quantification; see Equation 1.

$$\mathrm{LOD} = \frac{3.3\sigma}{\mathrm{s}} \qquad \mathrm{LOQ} = \frac{10\sigma}{\mathrm{s}} \tag{1}$$

3.8. Biological Assays

3.8.1. Cell Viability Assay

A preliminary assessment of the cytotoxicity of **HP1** and **HP6**-**HP8**, all of the isolated compounds **1**–**7**, and the found in **ZAP** from *H. palustris* on SCC-25 and normal fibroblast (PCS-201-012) cells using MTT (methyl thiazolyl tetrazolinum) was conducted according to Carmichael's method with some modifications [40]. The cell viability assay leans on the transformation of yellow tetrazolinum bromide MTT solution to the purple derivative of formazan via succinate dehydrogenase, an enzyme present in viable cells. Cells were cultured (1×10^4 per well) on a 96-well plate to receive 70% of their confluency. After 24 h and 48 h of incubation with the studied samples (prepared as DMSO solutions

directly before the assay), the cells were washed with PBS (phosphate-buffered saline). Subsequently, the MTT solution was added, and the plates were incubated at 37 °C for 2 h. Then, formazan crystals were dissolved in 200 µL of DMSO with Sorensen's glycine buffer and were shacked for 10 min. The absorbance was measured at a 570 nm wavelength using a microplate reader (EPOCH 2, BioTek, Winooski, VT, USA). The extracts and compounds were used at a final DMSO concentration of no more than 0.1% (*v*/*v*) in each well. The **HP1** and **HP6**-**HP8** extracts were analyzed at the following concentrations: 6.25–200 µg/mL, while compounds **1**–**7**, **ZAP** and **cPT** which was used as a positive control, were analyzed at 6.25–200 µM.

3.8.2. Proliferation Assay

The proliferation of the tested cells was estimated as [^{3}H]-thymidine incorporation into the DNA of the cells treated with the studied samples [40]. Firstly, cells (1×10^4 per well) were placed in 24-well plates and were allowed to adhere for 24 h. Afterwards, the cells were treated with 1 mL of growth medium containing 0.5 µCi [^{3}H]-thymidine and various concentrations of each sample (**HP1** and **HP6**-HP7; compounds **1** and **7**; and **ZAP**). **cPT** was used as a positive control. After incubation for 24 h and 48 h at 37 °C, the cells were rinsed with PBS and solubilized with 1 mL of 0.1 M NaOH (sodium hydroxide) containing 1% SDS (sodium dodecyl sulfate). Then, radioactivity was recorded in a Liquid Scintillation Analyzer (Perkin-Elmer, Waltham, MA, USA) after correction to 9 mL with scintillation liquid.

3.9. Statistical Analysis and Software

Mass Hunter Qualitative Analysis 10.0 (Agilent, Santa Clara, CA, USA) analysis was used to complete and process the chromatographic data. MS Excel 2016 with the Data Analysis add-on was used for statistical analysis and for regression calculation (Microsoft, Redmond, WA, USA). Linear regression parameters for the standard curve were determined using ANOVA. The IC_{50} and standard deviation values were calculated using GraphPad Prism 9 software (GraphPad Software, San Diego, CA, USA).

Supplementary Materials: The following supporting information can be downloaded at https://www.mdpi.com/article/10.3390/molecules27144415/s1: Table S1: Crystal data and structure refinement details for compounds **2**–**7**, Figure S1: Mass spectrum of compound **4** in negative ion mode (fragmentor = 320 V), Figure S2: UV spectrum of compound **4**, Figure S3: ^{1}H NMR spectrum (400 MHz) of compound **4** in $CDCl_3$, Figure S4: ^{13}C NMR spectrum (100 MHz) of compound **4** in $CDCl_3$, Figure S5: COSY spectrum of compound **4** in $CDCl_3$, Figure S6: ROESY spectrum of compound **4** in $CDCl_3$, Figure S7: HMBC spectrum of compound **4** in $CDCl_3$, Figure S8: HMQC spectrum of compound **4** in $CDCl_3$, Figure S9: UV spectrum of compound **5**, Figure S10: Mass spectrum of compound **5** in negative ion mode (fragmentor = 320 V), Figure S11: ^{1}H NMR spectrum (400 MHz) of compound **5** in $CDCl_3$, Figure S12: ^{13}C NMR spectrum (100 MHz) of compound **5** in $CDCl_3$, Figure S13: COSY spectrum of compound **5** in $CDCl_3$, Figure S14: ROESY spectrum of compound **5** in $CDCl_3$, Figure S15: HSQC spectrum of compound **5** in $CDCl_3$, Figure S16: HMBC spectrum of compound **5** in $CDCl_3$, Figure S17: Mass spectrum of compound **6** in negative ion mode (fragmentor = 180 V), Figure S18: UV spectrum of compound **6**, Figure S19: ^{1}H NMR spectrum (400 MHz) of compound **6** in DMSO-*d6*, Figure S20: ^{13}C NMR spectrum (100 MHz) of compound **6** in DMSO-*d6*, Figure S21: COSY spectrum of compound **6** in DMSO-*d6*, Figure S22: HMQC spectrum of compound **6** in DMSO-*d6*, Figure S23: HMBC spectrum of compound 6 in DMSO-*d6*, Figure S24: ROESY spectrum of compound **6** in DMSO-*d6*, Figure S25: Mass spectrum of compound **7** in negative ion mode (fragmentor = 180 V), Figure S26: UV spectrum of compound **7**, Figure S27: ^{1}H NMR spectrum (400 MHz) of compound **7** in DMSO-d6, Figure S28: ^{13}C NMR spectrum (100 MHz) of compound **7** in DMSO-*d6*, Figure S29: COSY spectrum of compound **7** in DMSO-*d6*; Figure S30: ROESY spectrum of compound **7** in DMSO-*d6*, Figure S31: HMBC spectrum of compound **7** in DMSO-*d6*,Figure S32: HSQC spectrum of compound **7** in DMSO-*d6*; Table S2: Main HPLC optimization method and validation parameters, Figure S33: UV–VIS chromatogram of separated compounds **1**–**7**

and **ZAP** obtained by HPLC-PDA, Figure S34: UV–VIS chromatogram of extracts **HP1** and **HP6–8** with well-separated compounds **1–7** and zapotin (**ZAP**) obtained by HPLC-PDA (345 *nm*).

Author Contributions: Conceptualization, J.W.S., K.J. and M.T.; methodology, J.W.S., Ł.S. and K.B; validation, J.W.S.; formal analysis, J.W.S., K.J. and K.B.; investigation, J.W.S., K.J., Ł.S., P.D. and K.B.; writing—original draft preparation, J.W.S. and K.J.; writing—review and editing, J.W.S. and M.T.; visualization, J.W.S. and K.J.; supervision, M.T. and J.A.P. All authors have read and agreed to the published version of the manuscript.

Funding: This study received funding from grant No. SUB/2/DN/22/003/2212.

Institutional Review Board Statement: Not applicable.

Informed Consent Statement: Not applicable.

Data Availability Statement: Data are contained within the article and in the Supplementary Materials. Further information is available upon request from the corresponding author.

Acknowledgments: The authors would like to thank J. Nazaruk for her kind help in collecting and identifying the plant material. Special thanks to Krzysztof Bielawski from the Medical University of Białystok for providing a laboratory to conduct the melting point study for the new compounds.

Conflicts of Interest: The authors declare no conflict of interest.

Sample Availability: Samples of compounds **1–7** are available from the authors.

Abbreviations

$[\alpha]_D$	Specific rotation at the sodium D line
$AlCl_3$	Aluminum chloride
ANOVA	Analysis of variance
c	Concentration
C8	Column contains octyl carbon chain bonded to silica
cPT	Cisplatin
$CDCl_3$	Deuterated chloroform
COSY	Correlation spectroscopy
DEPT	Distortionless enhancement by polarization transfer
DMSO	Dimethyl sulfoxide
DMSO-*d*6	Deuterated dimethyl sulfoxide
H_3BO_3	Boric acid
HCL	Hydrochloric acid
HMBC	Heteronuclear multiple bond correlation
HMQC	Heteronuclear multiple quantum coherence
HPLC-PDA	High-pressure liquid chromatograph with a photodiode array detector
HRMS	High-resolution mass spectrometry
HSQC	Heteronuclear single quantum coherence
IC_{50}	Median inhibitory concentration
LC-MS	Liquid chromatography coupled with mass spectrometry
LOD	Limit of detection
LOQ	Limit of quantification
LPLC	Low-pressure liquid chromatography
mp.	Melting point
MTT	Methyl thiazolyl tetrazolinum
NaOAc	Sodium acetate
NaOH	Sodium hydroxide
NaOMe	Sodium methoxide
NMR	Nuclear magnetic resonance
PBS	Phosphate-buffered saline
ROESY	Rotating-frame nuclear overhauser effect spectroscopy
SDS	Sodium dodecyl sulfate
UV–Vis	Ultraviolet-visible spectroscopy

References

1. Sung, H.; Ferlay, J.; Siegel, R.L.; Laversanne, M.; Soerjomataram, I.; Jemal, A.; Bray, F. Global Cancer Statistics 2020: GLOBOCAN Estimates of Incidence and Mortality Worldwide for 36 Cancers in 185 Countries. *CA. Cancer J. Clin.* **2021**, *71*, 209–249. [CrossRef] [PubMed]
2. Fridlender, M.; Kapulnik, Y.; Koltai, H. Plant derived substances with anti-cancer activity: From folklore to practice. *Front. Plant. Sci.* **2015**, *6*, 799. [CrossRef] [PubMed]
3. Seca, A.; Pinto, D. Plant secondary metabolites as anticancer agents: Successes in clinical trials and therapeutic application. *Int. J. Mol. Sci.* **2018**, *19*, 263. [CrossRef]
4. Forni, C.; Rossi, M.; Borromeo, I.; Feriotto, G.; Platamone, G.; Tabolacci, C.; Mischiati, C.; Beninati, S. Flavonoids: A myth or a reality for cancer therapy? *Molecules* **2021**, *26*, 3583. [CrossRef]
5. Khan, A.U.; Dagur, H.S.; Khan, M.; Malik, N.; Alam, M.; Mushtaque, M. Therapeutic role of flavonoids and flavones in cancer prevention: Current trends and future perspectives. *Eur. J. Med. Chem. Reports* **2021**, *3*, 100010. [CrossRef]
6. Ravishankar, D.; Rajora, A.K.; Greco, F.; Osborn, H.M.I. Flavonoids as prospective compounds for anti-cancer therapy. *Int. J. Biochem. Cell Biol.* **2013**, *45*, 2821–2831. [CrossRef] [PubMed]
7. Gutiérrez-Venegas, G.; Sánchez-Carballido, M.A.; Delmas Suárez, C.; Gómez-Mora, J.A.; Bonneau, N. Effects of flavonoids on tongue squamous cell carcinoma. *Cell Biol. Int.* **2020**, *44*, 686–720. [CrossRef] [PubMed]
8. Stanisław, K.; Grzegorz, K. *Flora Polski. Rośliny wodne i bagienne*; MULTICO Oficyna Wydawnicza: Warsaw, Poland, 2015.
9. Włodarczyk, M.; Pasikowski, P.; Osiewała, K.; Frankiewicz, A.; Dryś, A.; Gleńsk, M. In search of high-yielding and single-compound-yielding plants: New sources of pharmaceutically important saponins from the Primulaceae family. *Biomolecules* **2020**, *10*, 376. [CrossRef]
10. Ramesh, S.; Rajan, R.; Santhanam, R. *Freshwater Phytopharmaceutical Compounds*; CRC Press: Boca Raton, FL, USA, 2013.
11. Bach Original Flower Remedies. Available online: https://www.bachremedies.com/en-us/ (accessed on 17 May 2022).
12. Jakimiuk, K.; Sari, S.; Milewski, R.; Supuran, C.T.; Şöhretoğlu, D.; Tomczyk, M. Flavonoids as tyrosinase inhibitors in *in silico* and *in vitro* models: Basic framework of SAR using a statistical modelling approach. *J. Enzyme Inhib. Med. Chem.* **2022**, *37*, 427–436. [CrossRef]
13. Strawa, J.; Szoka, Ł.; Tomczyk, M. Preliminary studies of the chemical composition and cytotoxic activity of *Hottonia palustris* herb. *Planta Med.* **2019**, *85*, 1544. [CrossRef]
14. Strawa, J.W.; Galanty, A.; Jakimiuk, K.; Grabowska, K.; Tomczyk, M. Cytotoxic effect on human melanoma cell lines and tyrosinase inhibition of *Hottonia palustris*. *Planta Med.* **2021**, *87*, 1304. [CrossRef]
15. Zawadiak, J.; Mrzyczek, M. Correlation of substituted aromatic β-diketones' characteristic protons chemical shifts with Hammett substituent constants. *Magn. Reson. Chem.* **2013**, *51*, 689–694. [CrossRef] [PubMed]
16. Wojtulewski, S.; Strawa, J.W.; Tomczyk, M.; Gaweł, M.; Brzeziński, K. A new look at two polymorphic crystal structures of dibenzoylmethane: Relationship between the crystal packing and the hydrogen atom position revealed by quantum chemistry and quantum crystallography methods. *Acta Crystallogr. Sect. B Struct. Sci. Cryst. Eng. Mater.* **2020**, *B76*, 957–966. [CrossRef] [PubMed]
17. Shibata, S. Antitumor-promoting and anti-inflammatory activities of licorice principles and their modified compounds. In *Food Phytochemicals for Cancer Prevention II*; American Chemical Society: Washington, DC, USA, 1994; Volume 547, pp. 308–321.
18. Peng, Y.; Bishop, K.S.; Quek, S.Y. Compositional analysis and aroma evaluation of Feijoa essential oils from New Zealand grown cultivars. *Molecules* **2019**, *24*, 2053. [CrossRef]
19. Mabry, T.J.; Markham, K.R.; Thomas, M.B. *The systematic identification of flavonoids*; Springer: Berlin/Heidelberg, Germany, 1970.
20. Dias, M.C.; Pinto, D.C.G.A.; Silva, A.M.S. Plant flavonoids: Chemical characteristics and biological activity. *Molecules* **2021**, *26*, 5377. [CrossRef]
21. Nguyen, T.K.P.; Nguyen, K.P.P.; Kamounah, F.S.; Zhang, W.; Hansen, P.E. NMR of a series of novel hydroxyflavothiones. *Magn. Reson. Chem.* **2009**, *47*, 1043–1054. [CrossRef]
22. Ambrozin, A.R.P.; Vieira, P.C.; Fernandes, J.B.; Silva, M.F.d.G.F.d.; Albuquerque, S.d. New pyranoflavones and trypanocidal activity of compounds isolated from *Conchocarpus heterophyllus*. *Quim. Nova* **2008**, *31*, 740–743. [CrossRef]
23. Tokalov, S.V.; Kind, B.; Wollenweber, E.; Gutzeit, H.O. Biological effects of epicuticular flavonoids from *Primula denticulata* on human leukemia cells. *J. Agric. Food Chem.* **2004**, *52*, 239–245. [CrossRef]
24. Zakharov, A.M.; Glyzin, V.I.; Ban'kovskii, A.I. Flavonoids from *Primula turkestanica*. *Chem. Nat. Compd.* **1971**, *7*, 814. [CrossRef]
25. Boltenkov, E.V.; Rybin, V.G.; Zarembo, E.V. Flavones from callus tissue of *Iris ensata*. *Chem. Nat. Compd.* **2005**, *41*, 539–541. [CrossRef]
26. Wollenweber, E.; Iinuma, M.; Tanaka, T.; Mizuno, M. 5-Hydroxy-6,2′-dimethoxyflavone from *Primula denticulata*. *Phytochemistry* **1990**, *29*, 633–637. [CrossRef]
27. Somayaji, A.; Shastry, C.S. Interference of antioxidant flavonoids with MTT tetrazolium assay in a cell free system. *J. Pharm. Res. Int.* **2021**, 76–83. [CrossRef]
28. Habtemariam, S. Catechols and quercetin reduce MTT through iron ions: A possible artefact in cell viability assays. *Phyther. Res.* **1995**, *9*, 603–605. [CrossRef]
29. Strawa, J.W.; Jakimiuk, K.; Tomczyk, M. Zapotin, a polymethoxyflavone, with potential therapeutic attributes. *Int. J. Mol. Sci.* **2021**, *22*, 13227. [CrossRef] [PubMed]

30. Mohammed, H.A.; Abd El-Wahab, M.F.; Shaheen, U.; Mohammed, A.E.-S.I.; Abdalla, A.N.; Ragab, E.A. Isolation, characterization, complete structural assignment and anticancer activities of the methoxylated flavonoids from *Rhamnus disperma* roots. *Molecules* **2021**, *26*, 5827. [CrossRef]
31. Jackson, K.M.; DeLeon, M.; Verret, C.R.; Harris, W.B. Dibenzoylmethane induces cell cycle deregulation in human prostate cancer cells. *Cancer Lett.* **2002**, *178*, 161–165. [CrossRef]
32. Kopustinskiene, D.M.; Jakstas, V.; Savickas, A.; Bernatoniene, J. Flavonoids as anticancer agents. *Nutrients* **2020**, *12*, 457. [CrossRef]
33. Tutin, T.G.; Heywood, V.H.; Burges, N.A.; Moore, D.M.; Valentine, D.H.; Walters, S.M.; Webb, D.A. *Flora Europaea*; Cambridge University Press: Cambridge, UK, 1972.
34. Dolomanov, O.V.; Bourhis, L.J.; Gildea, R.J.; Howard, J.A.K.; Puschmann, H. OLEX2: A complete structure solution, refinement and analysis program. *J. Appl. Crystallogr.* **2009**, *42*, 339–341. [CrossRef]
35. Sheldrick, G.M. SHELXT-Integrated space-group and crystal-structure determination. *Acta Crystallogr. Sect. A Found. Adv.* **2015**, *71*, 3–8. [CrossRef]
36. Sheldrick, G.M. Crystal structure refinement with SHELXL. *Acta Crystallogr. Sect. C Struct. Chem.* **2015**, *71*, 3–8. [CrossRef] [PubMed]
37. Spek, A.L. Structure validation in chemical crystallography. *Acta Crystallogr. Sect. D Biol. Crystallogr.* **2009**, *65*, 148–155. [CrossRef] [PubMed]
38. Centre Cambridge Crystallographic Data The Cambridge Crystallographic Data Centre (CCDC). Available online: www.ccdc.cam.ac.uk/data_request/cif (accessed on 7 May 2022).
39. ICH Harmonised Tripartte Guideline Q2(R1) Validation of Analytical Procedures: Text and Methodology. Available online: https://database.ich.org/sites/default/files/Q2%28R1%29Guideline.pdf (accessed on 7 May 2022).
40. Szoka, L.; Nazaruk, J.; Stocki, M.; Isidorov, V. Santin and cirsimaritin from *Betula pubescens* and *Betula pendula* buds induce apoptosis in human digestive system cancer cells. *J. Cell. Mol. Med.* **2021**, *25*, 11085–11096. [CrossRef] [PubMed]